A Fabry–Pérot fiber-optic ultrasonic hydrophone for the simultaneous measurement of temperature and acoustic pressure

Paul Morris[a)]
Department of Medical Physics and Bioengineering, University College London, Gower Street, London WC1E 6BT, United Kingdom

Andrew Hurrell
Precision Acoustics Ltd., Hampton Farm Business Park, Higher Bockhampton, Dorchester DT2 8QH, United Kingdom

Adam Shaw
Quality of Life Division, National Physical Laboratory, Hampton Road, Teddington, Middlesex TW11 0LW, United Kingdom

Edward Zhang and Paul Beard
Department of Medical Physics and Bioengineering, University College London, Gower Street, London WC1E 6BT, United Kingdom

(Received 9 October 2008; revised 11 March 2009; accepted 16 March 2009)

A dual sensing fiber-optic hydrophone that can make simultaneous measurements of acoustic pressure and temperature at the same location has been developed for characterizing ultrasound fields and ultrasound-induced heating. The transduction mechanism is based on the detection of acoustically- and thermally-induced thickness changes in a polymer film Fabry–Pérot interferometer deposited at the tip of a single mode optical fiber. The sensor provides a peak noise-equivalent pressure of 15 kPa (at 5 MHz, over a 20 MHz measurement bandwidth), an acoustic bandwidth of 50 MHz, and an optically defined element size of 10 μm. As well as measuring acoustic pressure, temperature changes up to 70 °C can be measured, with a resolution of 0.34 °C. To evaluate the thermal measurement capability of the sensor, measurements were made at the focus of a high-intensity focused ultrasound (HIFU) field in a tissue mimicking phantom. These showed that the sensor is not susceptible to viscous heating, is able to withstand high intensity fields, and can simultaneously acquire acoustic waveforms while monitoring induced temperature rises. These attributes, along with flexibility, small physical size (OD ~ 150 μm), immunity to Electro-Magnetic Interference (EMI), and low sensor cost, suggest that this type of hydrophone may provide a practical alternative to piezoelectric based hydrophones.
 [DOI: 10.1121/1.3117437]

PACS number(s): 43.35.Yb, 43.35.Wa, 43.30.Xm [TDM] Pages: 3611–3622

I. INTRODUCTION

Ultrasonic hydrophones are widely used to characterize diagnostic and therapeutic medical ultrasound fields. In both cases there are stringent measurement requirements to be met.[1] The increasing prevalence of higher frequency ultrasound in diagnostic imaging devices, such as very high frequency ocular and intravascular scanners, calls for measurement bandwidths that extend to several tens of megahertz. In addition, to minimize spatial averaging errors at these frequencies, an element size smaller than the acoustic wavelength ($\approx$75 μm at 20 MHz in water) is desirable. Although piezoelectric polyvinylidene (PVdF) needle and membrane hydrophones can readily meet the bandwidth requirement, achieving element sizes on this scale with adequate sensitivity is problematic as sensitivity decreases with decreasing element area.

Characterizing therapeutic ultrasound fields poses a somewhat different measurement challenge. The hydrophone bandwidth and element size requirements are often less demanding than for diagnostic ultrasound measurements since the fundamental frequencies used tend to be in the low megahertz range. The greater challenge lies in withstanding the hostile environment that can be produced, particularly where high amplitude or high intensity focused beams are employed, such as in extracorporeal lithotripsy or high-intensity focused ultrasound (HIFU) therapy. In the latter case, for example, the cavitational activity and temperature rises induced at clinical intensities can readily damage PVDF hydrophones. A further requirement for procedures that exploit thermal effects to provide a therapeutic benefit is measurement of the induced temperature rise within the sound field. This is most commonly achieved using wire thermo-

[a)]Author to whom correspondence should be addressed. Electronic mail: psmorris@medphys.ucl.ac.uk

couple probes. These are acoustically robust, sensitive, and small enough to be inserted into tissue or a tissue mimicking phantom for *in-situ* measurements.[2,3] However, they can suffer from significant measurement errors due to viscous self-heating induced by the ultrasound field.[4] Although the thin-film thermocouple[5–7] does not suffer from this limitation, its large size prevents it from being used *in-situ*. Furthermore, it is fragile and susceptible to damage by high intensity fields. It would also be advantageous if both the temperature rise and the acoustic pressure could be measured simultaneously at the same location. This would enable the two measurands to be correlated in order to study the relationship between acoustic and thermal effects, for example, to elucidate the role that cavitation plays in enhancing heating in HIFU therapy. To our knowledge, this type of dual measurement capability has not previously been demonstrated using non-optical methods.

Fiber optic hydrophones offer the prospect of overcoming some or all of the above limitations. The most practically applicable type of fiber-optic hydrophone is the extrinsic type. This employs a fiber-optic downlead to deliver light to and from an optical sensor, or some transducing mechanism, at the end of the fiber. In principle, the sensitive region is defined by the spot size of the incident illumination. This, in turn, is given by the fiber core diameter which is typically a few microns for a single mode optical fiber. This offers the prospect of providing acoustically small element sizes at frequencies of tens of megahertz. Other generic advantages include the small fiber diameter (≈ 150 μm), a flexible probe type configuration, robustness, low cost, immunity to EMI, and in some cases the ability to measure temperature as well as pressure. Several types of extrinsic fiber-optic hydrophone have been investigated for measurement applications in medical ultrasound. The simplest is based on the detection of pressure-induced changes in the Fresnel reflection coefficient at the tip of an optical fiber.[8–11] This approach offers very low sensor cost, technical simplicity, and the potential for exceptionally wide bandwidth, limited by the wavelength of light and thus potentially extending to several hundred megahertz. Furthermore, there is the potential to measure ultrasound-induced heating since the Fresnel reflection coefficient is dependent on temperature as well as pressure. The fundamental disadvantage, however, is low acoustic sensitivity with a broadband noise-equivalent-pressure (NEP) typically of the order of 1 MPa. This limits its application to the measurement of temporally stable signals that can be signal averaged over many cycles or the output of high amplitude sources, such as shockwave lithotripters.[9,12,13]

Higher detection sensitivities, comparable to those of PVDF hydrophones, have been obtained by exploiting interferometric methods. A promising approach that has been explored for medical ultrasound metrology is based on the detection of acoustically-induced changes in the optical thickness of a solid Fabry–Pérot interferometer (FPI) located at the tip of an optical fiber. Two variants of this approach, distinguished by the materials and methods used to fabricate the FPI, have been demonstrated. One involves sputtering onto the fiber tip, a multilayer dielectric sensing structure comprising a central SiO_2 spacer sandwiched between two stacks of alternating SiO_2 and Nb_2O_5 layers—the latter form the mirrors of the FPI.[14] The small thickness of the multilayer structure (typically a few microns) enables bandwidths extending to several hundred megahertz to be achieved.[15] Although this type of sensor has not been evaluated for the purpose of measuring ultrasound-induced heating, its potential for measuring temperature has been demonstrated by detecting laser-induced thermal transients.[16] The second approach employs a different design, one in which the spacer between the two FPI mirrors is a polymer.[17–20] The lower Young modulus of polymers compared to relatively hard dielectrics such as SiO_2 results in larger acoustically-induced phase shifts and thus higher sensitivity for a given FPI finesse.[21] The thickness of the spacer tends to be larger (10–100 μm) than the SiO_2 spacer referred to above providing bandwidths in the tens of megahertz range. It also results in a smaller free spectral range, thereby reducing the required wavelength tuning range for the interrogating laser. An early laboratory prototype hydrophone system based on this type of sensor has been demonstrated previously.[20] This system employed a free space 850 nm distributed Bragg reflector (DBR) laser diode as the interrogation source (the wavelength of which was manually adjusted in order to optimally bias the FPI) and provided a bandwidth of 25 MHz and a peak NEP of 10 kPa (over a 25 MHz measurement bandwidth). This type of sensor has also been used to detect laser-induced thermal transients[22] and a preliminary study has been undertaken to evaluate its ability to measure ultrasound-induced heating.[23]

In this paper, we provide a detailed account of a system based on this approach but incorporating several key technical developments. These include modifying the design of the sensor and the system detection optoelectronics to extend the acoustic bandwidth to 50 MHz and the use of a computer controlled discretely tunable "telecom" laser to interrogate the sensor. The latter significantly enhances the practical utility of the concept as it enables the FPI biasing procedure to be fully automated. Furthermore, because the laser is fiber-coupled, stability problems associated with coupling free-space beams into single mode fibers are eliminated. A major advance has been the development and implementation of a sensor interrogation algorithm that enables simultaneous measurements of temperature and acoustic pressure to be made for the first time.

Section II A describes the acoustic and thermal transduction mechanisms of the sensor and the interrogation scheme used to recover pressure and temperature simultaneously. Sections II B–II D describe the procedure used to fabricate the sensor, the design of the instrumentation required to interrogate it, and the practical implementation of the interrogation scheme. In Sec. III, the acoustic performance in terms of sensitivity, linearity, frequency response, and directivity are discussed, and in Sec. IV the thermal sensitivity and response time are described. The dual measurement capability of the system, demonstrated by making measurements of ultrasound-induced heating in a tissue phantom, is discussed in Sec. V.

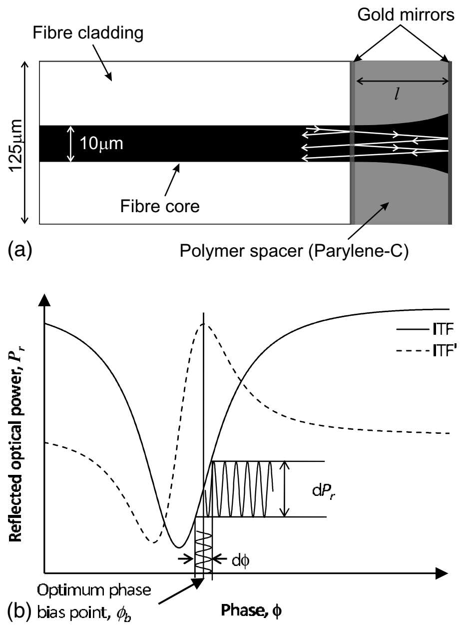

FIG. 1. (a) Schematic of FPI sensor. (b) Phase (ITF) and its first derivative (ITF′). Operation at optimum phase bias point ϕ_b for the linear detection of a small acoustically-induced phase modulation $d\phi$ is illustrated.

II. THE FABRY–PÉROT FIBER OPTIC HYDROPHONE

A. Principles of operation

A schematic of the tip of the fiber-optic hydrophone is shown in Fig. 1(a). The sensing element is a FPI which comprises a thin ($l \approx 10$ μm) Parylene-C polymer film spacer sandwiched between a pair of gold mirrors. Light emitted by a tunable laser is incident on the FPI and is multiply reflected from both mirrors and interferes as it re-enters the fiber. Acoustically- or thermally-induced changes in the optical thickness of the polymer spacer produce a corresponding phase shift between the light reflected from the two mirrors. This is demodulated to obtain a measure of pressure or temperature. In Secs. II A 1 and II A 2, the transduction mechanisms for each measurand are described.

1. Acoustic transduction mechanism

The variation in reflected optical power, P_r, from a FPI as a function of phase ϕ is termed the phase interferometer transfer function (ITF) where ϕ is given by

$$\phi = \frac{4\pi n l}{\lambda}, \tag{1}$$

where n and l are the refractive index and thickness of the polymer spacer, respectively, and λ is the optical wavelength. For a plane parallel FPI formed with non-absorbing mirrors and illuminated with a collimated beam, the phase ITF takes the form of the Airy function, an example of which is shown in Fig. 1(b) along with its derivative. In order to make an acoustic measurement, the laser wavelength is adjusted so that $\phi = \phi_b$, where ϕ_b is the phase corresponding to the peak derivative of the phase ITF. At this wavelength, the sensitivity and linearity are at a maximum and the FPI is said to be optimally biased. Under these conditions, a small acoustically-induced phase shift $d\phi$ can be regarded as being linearly converted to a corresponding change in the reflected optical power, dP_r.

The sensitivity, the reflected optical power modulation per unit acoustic pressure, at ϕ_b is given by

$$\frac{dP_r}{dp} = \frac{dP_r}{d\phi}\frac{d\phi}{dp}, \tag{2}$$

where p is the acoustic pressure. $dP_r/d\phi$ is the first derivative of the ITF at ϕ_b and is termed the optical phase sensitivity. It is dependent on the incident optical power and the finesse of the FPI. The finesse is in turn defined by the mirror reflectivities and the phase dispersion due to the divergence of the incident beam and non-uniformities in the spacer thickness.

$d\phi/dp$ is termed the acoustic phase sensitivity and represents the magnitude of the optical phase shift produced per unit pressure. The change in phase arises from a change in the optical thickness of the spacer and may be caused by two mechanisms, a change in physical thickness or a change in refractive index. In general, the acoustic phase sensitivity can be written as

$$\frac{d\phi}{dp} = \frac{4\pi}{\lambda}\left(n_0\frac{dl}{dp} + l\frac{dn}{dp}\right)P_l(k), \tag{3}$$

where dl is a small change in the spacer thickness and dn is a small change in the refractive index. $P_l(k)$ is a frequency modifying term that accounts for the spatial variation of stress within the spacer that occurs when an acoustic wave is incident on the sensor and is dependent on the geometry, structure, and physical properties of the fiber tip.[24] Equation (3) indicates that $d\phi/dp$ depends on the elasto-mechanical and elasto-optic properties of the spacer, although for the polymer (Parylene-C) spacers used in the sensors described in this study, the elasto-optic effect can be neglected.[25] Equation (3) can therefore be written as

$$\frac{d\phi}{dp} = \frac{4\pi n}{\lambda}\frac{l}{E}P_l(k), \tag{4}$$

where E is the Young modulus of the spacer. Equation (4) shows that the sensitivity is proportional to the thickness of the spacer and inversely proportional to the Young modulus of the material. Thus a sensor with a thicker spacer will have a higher sensitivity but reduced bandwidth since the sensor responds to the spatial average of the stress over its sensitive volume.

2. Thermal transduction mechanism

When subjected to a change in temperature, the optical thickness of the FPI spacer will change due to thermal expansion and the change in refractive index (the thermo-optic effect). In principle, the resulting phase shift could be recovered by optimally biasing the FPI and measuring the reflected optical power modulation as described in Sec. II A 1. Indeed, such an approach has been employed previously to make temperature measurements using FPIs.[16,22,26,27] However, this method has several limitations. First, it is expected that for a polymer spacer, even a relatively small temperature change of only few degrees will induce a phase shift that

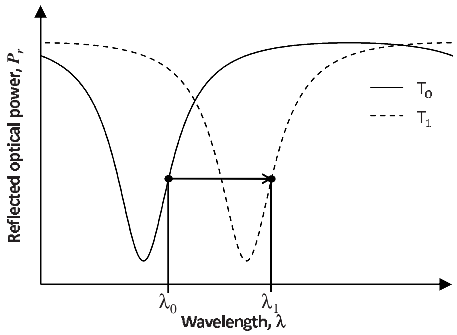

FIG. 2. Effect of temperature on the wavelength ITF. A change in temperature from T_0 to T_1 produces a linear shift in the optimum bias wavelength from λ_0 to λ_1.

exceeds the phase range over which the ITF is linear around the optimum bias point ϕ_b. As well as compromising the linearity of the temperature measurement, a phase shift of this magnitude will shift the bias point to the extent that it no longer corresponds to the peak derivative of the ITF thus reducing the acoustic sensitivity. This will clearly be problematic if simultaneous acoustic and temperature measurements are required. In addition, unlike acoustic measurements, the relatively long timescale (milliseconds to seconds) of thermal excursions makes temperature measurements susceptible to low frequency noise such as that due to fluctuations in the laser output power. For these reasons, the following alternative interrogation scheme which relies on tracking the optimum bias wavelength has been implemented.

Figure 2 shows the reflected optical power as a function of wavelength. This is termed the wavelength interferometer transfer function. At temperature T_0, an optimum bias wavelength, λ_0, can be found which corresponds to ϕ_b, the phase bias at the peak derivative of the phase ITF in Fig. 1(a). Thus we can write

$$\phi_b = \frac{4\pi(nl)_0}{\lambda_0}, \tag{5}$$

where $(nl)_0$ is the optical thickness at temperature T_0. If the wavelength ITF is measured at a different temperature, T_1, a different wavelength, λ_1, is now found to correspond to ϕ_b and we can write

$$\phi_b = \frac{4\pi(nl)_1}{\lambda_1}, \tag{6}$$

where $(nl)_1$ is the optical thickness at T_1. From Eqs. (5) and (6), it can be seen that the change in the optimum bias wavelength, $\Delta\lambda=\lambda_1-\lambda_0$, which occurs for a temperature change $\Delta T=T_1-T_0$, is given by

$$\Delta\lambda = \frac{4\pi}{\phi_b}\Delta(nl), \tag{7}$$

where $\Delta(nl)$ is the change in optical thickness caused by the temperature change. Providing $\Delta(nl)$ is directly proportional to the change in temperature, the shift in the optimum bias wavelength will also be proportional to the temperature change. This wavelength shift could, in principle, be measured by continually sweeping the laser wavelength and tracking the wavelength ITF as it shifts along the horizontal axis with temperature. If temperature alone is being measured, this approach would be feasible provided that the time to sweep the laser wavelength is small compared to the timescale of the temperature change. However, since the FPI is only transiently at the optimum phase bias point, ϕ_b, it would be difficult to make simultaneous ultrasound measurements with this method.

For this reason, an alternative interrogation scheme was developed. This requires initially tuning the laser output to the optimum bias wavelength and thereafter continuously monitoring the reflected optical power P_r. As soon as P_r changes due to a temperature-induced phase shift, the laser wavelength is immediately re-tuned so as to return P_r to its initial value. By continually re-adjusting the laser wavelength to maintain a constant P_r, the thermally-induced shift in the optimum bias wavelength, and therefore the temperature change, can be tracked over time. Providing the laser wavelength is rapidly re-tuned (before the thermally-induced phase shift becomes appreciable), the system will always be operating at, or close to, ϕ_b thus allowing an acoustic measurement to be made. In this way ultrasound waveforms can be acquired at the same time that the temperature is being monitored.

The sensitivity of the temperature change measurement using this method is dependent on several factors: first, the thermo-mechanical and thermo-optic properties of the Parylene spacer. The phase change, $d\phi$, induced by a temperature change, dT, can be written as

$$\frac{d\phi}{dT} = \frac{4\pi l}{\lambda}\left(n_0\alpha + \frac{dn}{dT}\right), \tag{8}$$

where α is the coefficient of (linear) thermal expansion and n_0 is the refractive index at T_0. For Parylene-C,[28] $\alpha=3.5\times10^{-5}\ {}^\circ\mathrm{C}^{-1}$ but no data exist for the thermo-optic coefficient dn/dT. However, Zhang *et al.*[29] proposed an empirical formula for the calculation of dn/dT of polymers based on the value of α. Using this, a value of $6\times10^{-5}\ {}^\circ\mathrm{C}^{-1}$ is obtained. Unlike the elasto-optic effect, the thermo-optic cannot therefore be neglected. Second, the optical phase sensitivity $(dP_r/d\phi)$ influences the thermal sensitivity since it defines the minimum detectable reflected power variation, which is used to determine when it is necessary to re-tune the laser to maintain a constant P_r. In addition, the minimum detectable temperature change depends on the wavelength tuning resolution of the laser.

B. Sensor fabrication

The sensors were fabricated in batches of 32 as follows. A 2 m length of 1550 nm single mode optical fiber (outer diameter of 125 μm and core diameter of 9 μm) is cleaved using an ultrasonic fiber cleaver (PK technology FK11). The fibers are then loaded into a mount for the deposition of the reflective coatings and polymer spacer. Thin gold films are used for the reflective coatings, with the reflectivity of the coating being controlled by the thickness of the film. A numerical model of the ITF was developed in order to inform

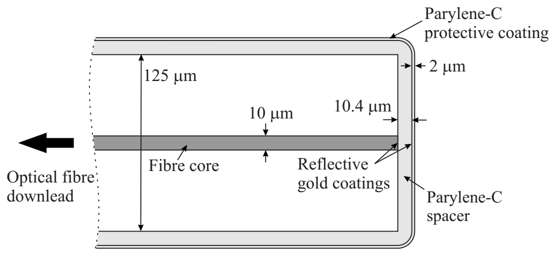

FIG. 3. Schematic of the FPI sensing structure deposited at the tip of the optical fiber.

the choice of mirror reflectivity.[24] It was found that a front mirror reflectivity of approximately 75% and a back mirror reflectivity of 98% (the maximum achievable with gold between 1500 and 1600 nm) were optimal. The gold coatings are deposited onto the tip of the optical fiber via a standard dc sputtering process. The polymer spacer was formed by vapor deposition of Parylene-C, poly(chloro-*para*-xylene).[20] Sensors were fabricated according to the process outlined above with a spacer thickness of 10.4 μm. In order to protect the sensing element, a second Parylene layer 2 μm thick was deposited over the tip of the fiber, as shown in Fig. 3.

There are several advantages of the above fabrication process. The use of a vapor phase deposition process to form the polymer spacer enables a highly conformal coating with excellent surface finish, good optical clarity, and uniformity of thickness to be achieved. These attributes allow a high quality FPI with good fringe visibility and finesse to be produced. The thickness can also be precisely controlled (<0.1 μm) to design sensors with specific free spectral ranges and acoustic bandwidths. Furthermore, the use of all vacuum deposition methods allows batch fabrication of large quantities of sensors with high repeatability at low unit cost.

C. The interrogation unit

Figure 4(a) shows a schematic of the system used to interrogate the sensor. The components within the dotted box make up the interrogation unit which has been developed into a fully integrated portable prototype [Fig. 4(b)]. The sensor downlead is terminated with an FC/APC connector which is inserted in the front panel of the interrogation unit. Light from a tunable laser is delivered to the downlead by means of a 2×2 fiber-optic coupler. Light reflected from the FPI is then routed to an InGaAs photodiode again via the coupler. A second photodiode is used to monitor the direct output from the laser. The photodiode measuring the light reflected from the sensor has both ac and dc coupled outputs. The dc coupled output is connected to an analog to digital data acquisition device which is connected to a control personal computer (PC) via a universal serial bus (USB) interface. This allows measurement of the reflected optical power from the sensor in order to measure the ITF and monitor temperature changes. The ac coupled output (-3 dB cut-off frequency: 50 kHz) is connected to an oscilloscope for measurement of acoustic waveforms.

The laser used in the system is an AltoWave 1100 tunable laser from Intune Technologies Ltd. The laser has a 40 nm tuning range in the telecoms C-band (1528–1568 nm)

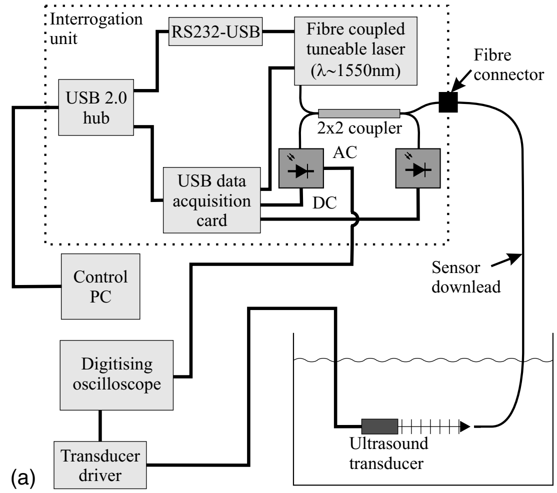

(a)

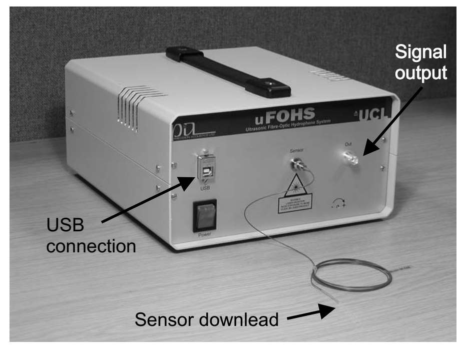

(b)

FIG. 4. (a) Schematic of the fiber-optic hydrophone system. The components contained in the dotted box form the interrogation unit shown in the photograph (b).

and is based on the sampled-grating (SG) DBR design. SG-DBR lasers are monolithically integrated semiconductor lasers and have no moving parts. This allows rapid, electronic wavelength tuning which is controlled via an RS232 communications interface. The AltoWave 1100 has an optical output power of approximately 8 mW, which is constant over its tuning range (±0.2 dB). It is tunable over 600 discrete wavelength channels, separated by a constant optical frequency of 8.33 GHz (≈0.06 nm increment in wavelength) and can perform a linear sweep through all 600 channels in a time of 120 ms. It is also capable of random channel to channel tuning in approximately 200 μs although in practice this is limited to approximately 2 ms due to the time taken to communicate with the PC via the RS232 interface.

D. Implementation of sensor biasing scheme

The following describes the practical implementation of the interrogation schemes described in Secs. II A 1 and II A 2.

1. Acoustic measurement

To acquire an acoustic waveform, it is necessary to bias the FPI, as described in Sec. II A 1. In principle, this can be achieved by sweeping the laser through its 40 nm wavelength range and measuring the reflected optical power P_r. Since the laser channels are separated by a constant optical

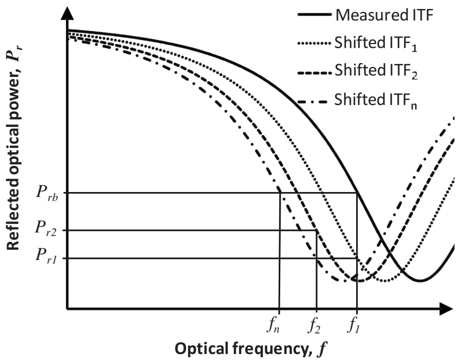

FIG. 5. Iterative scheme to optimally bias the FPI in the presence of self-heating.

frequency, and frequency is proportional to phase, plotting P_r as a function of channel provides a direct measure of the phase ITF. The latter can then be differentiated and the laser can be tuned to the wavelength that corresponds to the peak phase derivative. However, it was found that this approach was compromised by the heating of the FPI due to absorption of the laser light. This self-heating effect corrupts the measurement of the ITF since the optical thickness of the FPI varies during the wavelength sweep. To mitigate this, the ITF was obtained as rapidly as possible by performing a single sweep through the 40 nm wavelength range of the laser at the maximum tuning speed. Since the FPI is illuminated for only 120 ms, the self-heating is negligible enabling an accurate measurement of the ITF to be obtained. However, a difficulty was then found to arise when the laser wavelength was subsequently tuned to the optimum bias point. The FPI is now illuminated for an extended period and this results in a temperature rise large enough to cause the ITF to shift. The FPI is then no longer optimally biased.

To overcome this, an alternative interrogation scheme that relies on iteratively tuning the laser wavelength in order to search for P_{rb}, the reflected optical power at the optimum bias point, was implemented. This procedure is illustrated in Fig. 5. First, the ITF is measured by sweeping the laser through its 40 nm tuning range sufficiently quickly that significant self-heating does not occur as described above. From the ITF measured in this way (denoted "Measured ITF" in Fig. 5), the frequency f_1 and reflected power P_{rb} corresponding to the optimum bias point are identified. The laser frequency is then tuned to f_1. As a consequence, the reflected power measured by the photodiode is momentarily equal to P_{rb}. However, self-heating at f_1 immediately causes the ITF to shift, (becoming "shifted ITF$_1$") and so the reflected power now decreases from P_{rb} to P_{r1}. In an attempt to return the reflected power to P_{rb}, the laser is tuned to f_2. This results in a further (but smaller) shift in the ITF which now becomes "shifted ITF$_2$." At f_2, the reflected power P_{r2} is still less than P_{rb} so the laser is tuned yet again in order to approach P_{rb}. This procedure is repeated a number of times. With each iteration, the additional temperature rise due to self-heating becomes progressively smaller and therefore so too does the shift in the ITF. Eventually, after n iterations, the FPI attains a constant temperature, the position of the ITF no longer changes, and the system converges on P_{rb} which corresponds to the optimum bias point f_n. In practice, the iteration is terminated when the measured reflected optical power lies within 2% of the value obtained in the previous iteration. The system is then ready to make an acoustic measurement. The entire procedure including acquiring the ITF takes approximately 1 s. In practice, this procedure is implemented as an initialization routine when the system is switched on. Thereafter, the reflected power is monitored and if it changes by more than 2% the laser is retuned so as to maintain a constant value of P_r.

2. Temperature measurement

Assume that the system has been optimally biased as described above and that the sensor is now subjected to an external source of heat which produces a temperature rise over some time interval. As the temperature begins to increase, the reflected power P_r will change. If P_r changes by more than a small amount (2%), the laser wavelength is automatically adjusted by the control software so as to return P_r to P_{rb}, thus returning the system to the optimum bias point. As the temperature continues to rise, this procedure is repeated. In this way, the time course of the temperature rise is discretely sampled by tracking the changes in the bias wavelength as described in Sec. II A 1. Since the FPI is always maintained at the optimum bias point, ultrasound waveforms can be acquired at the same time the temperature is being monitored.

III. ACOUSTIC CHARACTERISTICS

The acoustic performance of the sensor was measured using a substitution calibration method[30] at Precision Acoustics Ltd., Dorchester, UK. This was carried out using a calibrated 0.4 mm (diameter) PVDF membrane hydrophone (Precision Acoustics Ltd., Dorchester, UK) that acted as a reference against which the fiber-optic hydrophone measurements were compared. The acoustic field was generated in water by a 1 MHz planar transducer producing a 25 cycle tone burst with an approximate peak to peak pressure of 1 MPa at the transducer face. Due to the non-linear propagation of the acoustic field in the water tank, integer harmonics of the fundamental up to at least 60 MHz are generated. This arrangement was used to measure the sensitivity, frequency response, and directivity of the hydrophone.

A. Sensitivity

Figure 6 shows a typical measurement of the shocked wave tone-burst as measured by both the reference membrane hydrophone [Fig. 6(a)] and the fiber-optic hydrophone [Fig. 6(b)]. In both cases the signals were acquired without signal averaging. The calibration sensitivities of the membrane hydrophone and fiber-optic hydrophone were 50 and 580 mV/MPa, respectively, at 5 MHz. Comparison of the signals shows that the signal-to-noise ratio of the fiber-optic hydrophone is comparable to that of the membrane hydrophone. The comparison also reveals significant structure in the signal from the fiber-optic hydrophone; this is due to the probe-type geometry of the sensor that causes radial resonances and edge waves that propagate across the tip of the

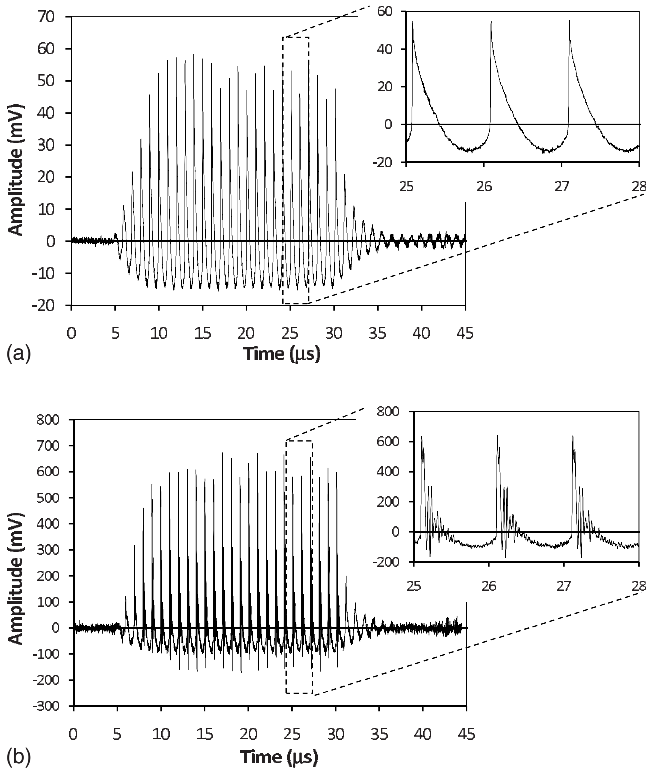

FIG. 6. Comparisons of the outputs of (a) a 0.4 mm PVDF membrane hydrophone and (b) the fiber-optic hydrophone in response to a "shocked" 1 MHz toneburst. Insets show expanded timescale (in μs).

fiber. These are then detected by the sensor as they cross the active area after the initial acoustic wave has passed. This will be described in more detail in Sec. III C.

The NEP, is defined as the acoustic pressure which provides a signal to noise ratio of 1. The NEP was obtained by recording the output of the photodiode over a 20 MHz bandwidth in the absence of an acoustic signal. The rms value of the noise voltage was then computed and multiplied by a factor of 3 to obtain the peak value. The peak noise voltage was then converted to an equivalent pressure by dividing by the calibration sensitivity (580 mV/MPa) of the hydrophone. This gave a peak NEP of 15 kPa (at 5 MHz) over a 20 MHz measurement bandwidth. By comparison, the peak NEP of the membrane hydrophone was 10 kPa and that of a 75 μm PVDF needle hydrophone (Precision Acoustics Ltd.) was 28 kPa under the same measurement conditions. Note that the peak rather than rms noise figures are quoted since the former provides a more realistic indication of the smallest signal that can be detected when measuring broadband signals in the time domain.

B. Linearity

Assuming the elastic limits of the polymer spacer are not exceeded, the upper limit of linear acoustic detection is determined by the phase range over which the gradient of the ITF is nearly constant at the bias point and the acoustic phase sensitivity. The linearity is determined by calculating the equation of the straight line which passes through the optimum bias point with a gradient equal to the peak derivative of the phase ITF. The difference between the ITF and the straight line is then calculated and the range of phase over which the difference is less than 5% and 10% determined.[20] The linear pressure range is then given by multiplying this phase range by the acoustic phase sensitivity. A value for the latter has been determined experimentally in a previous study.[20] This was found to be 0.075 rad/MPa for a sensor with a film thickness of 25 μm at a laser wavelength of 850 nm. Since $d\phi/dp$ is proportional to l/λ, this must be converted to the appropriate value for a sensor 10 μm in thickness interrogated by a laser wavelength of 1550 nm. The acoustic sensitivity can be found from

$$\left(\frac{\delta\phi}{\delta p}\right)_{(\lambda_2,l_2)} = \left(\frac{\delta\phi}{\delta p}\right)_{(\lambda_1,l_1)} \left(\frac{\lambda_1}{l_1}\right)\left(\frac{l_2}{\lambda_2}\right). \tag{9}$$

Noting that, in this case $\lambda_1=850$ nm, $\lambda_2=1550$ nm, $l_1=25$ μm, and $l_2=10$ μm, give

$$\left(\frac{\delta\phi}{\delta p}\right)_{(1550\ \text{nm},10\ \mu\text{m})} = 0.016\ \text{rad/MPa}. \tag{10}$$

The linear pressure range (to within 5%) of the fiber-optic hydrophone used to obtain the waveform shown in Fig. 6(b) is -4 MPa to 7.5 MPa. If a reduced linearity of 10% can be tolerated, this range becomes -6 MPa to 10 MPa. The pressure range is not symmetric as the ITF is not symmetrical about the bias point. The ITF reflectance minimum is also asymmetric, due to the use of metallic reflective coatings in the FPI. These metallic coatings introduce additional phase changes on reflection and transmission leading to the asymmetry in the ITF. As a result, the peak positive phase derivative is smaller than the peak negative derivative.

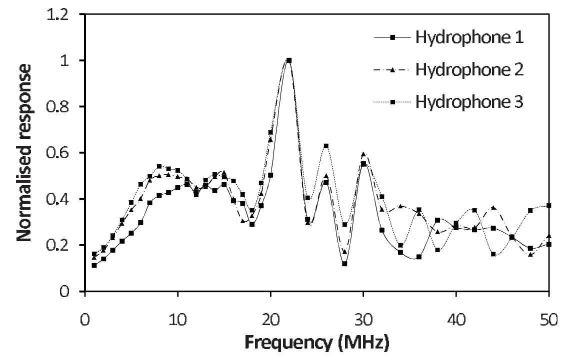

FIG. 7. Measured frequency responses of three typical fiber-optic hydrophones.

C. Frequency response

Figure 7 shows the frequency responses of three nominally identical fiber-optic hydrophones—the responses are normalized for ease of comparison. The calibration sensitivities of each hydrophone (hydrophones 1–3) at 5 MHz are 209, 255, and 580 mV/MPa, respectively—the variation in sensitivity is due to the fact that the output power of the laser was set to a different value for each hydrophone. The uncertainties associated with these measurements are as follows: 1–15 MHz, 14%; 16–20 MHz, 18%; 22–30 MHz, 23%; and 30–50 MHz, 40%, based on combined systematic and random uncertainties. It should be noted that the frequency re-

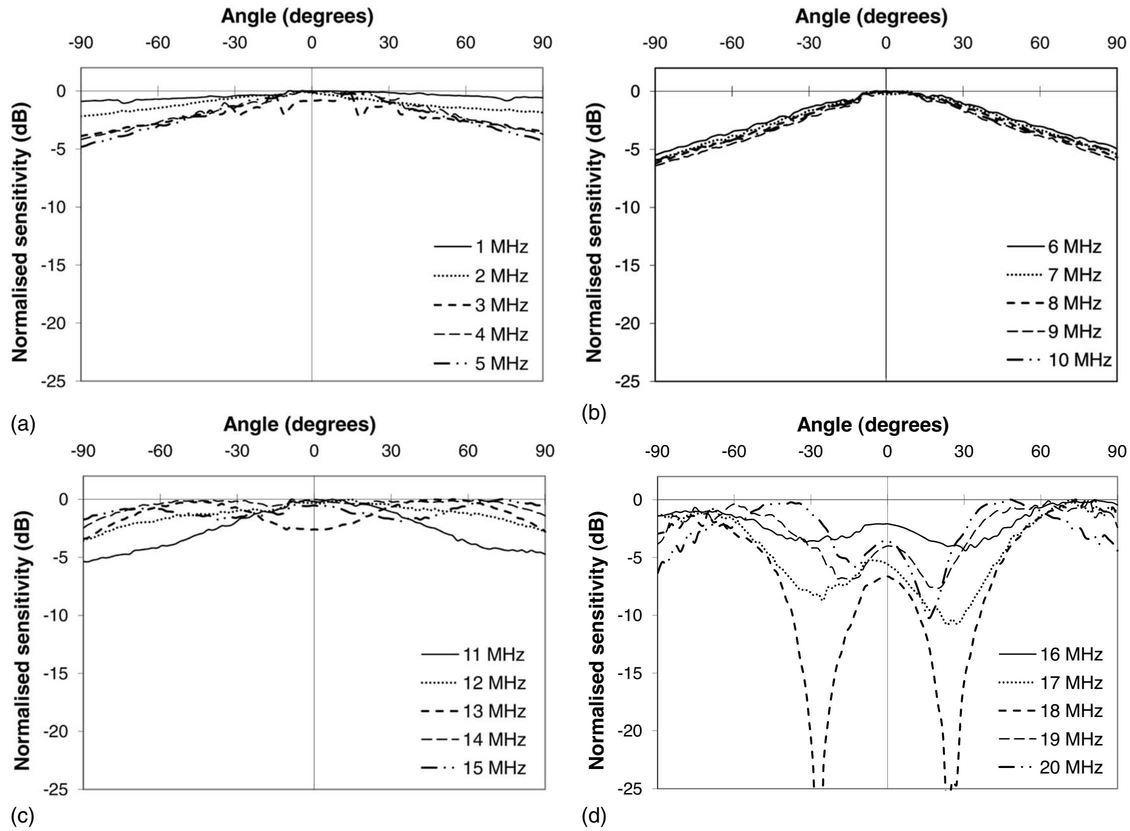

FIG. 8. Directional response of a fiber-optic hydrophone. Response shown for frequencies: (a) 1–5 MHz, (b) 6–10 MHz, (c) 11–15 MHz, and (d) 16–20 MHz.

sponses shown in Fig. 7 are those of the hydrophone system and thus include the finite bandwidth of the photodiodes (-3 dB bandwidth $\approx$50 MHz). Thus, while the response of the hydrophone decreases toward 50 MHz, the intrinsic response of the sensors is expected to extend beyond this. The responses of all three sensors are in close agreement up to 25 MHz indicating good sensor-to-sensor uniformity. Above this frequency, there is greater variation which is consistent with the higher uncertainty in the measurement. The variation may also be due to small differences in the geometries of the fiber tips, which will have greater influence at higher frequencies.

Figure 7 also shows that the frequency response of the hydrophone is significantly non-uniform. A detailed investigation of the frequency response, including a comparison using a finite difference simulation, has shown that the non-uniformities in the response arise from diffraction of the acoustic wave at the tip of the sensor.[24] The diffraction causes multiple edge waves to propagate and reverberate across the tip of the sensor. The presence of two diffracting boundaries (that of the fused silica fiber and Parylene spacer) leads to waves propagating with more than five different wave speeds: longitudinal in water, longitudinal and shear in the Parylene, and longitudinal and shear in the fused silica fiber as well as several interface wavespeeds. It is the frequency dependent interaction of all of these waves that is responsible for the complex structure in the frequency response.

D. Directivity

The directional response of a fiber-optic hydrophone was measured up to a frequency of 20 MHz at 1 MHz intervals, as shown in Fig. 8. The multitude of wave types that interact within the sensor and contribute to its output means that the directivity inevitably differs from that of an ideal rigid disk receiver. It can be seen that for frequencies up to 10 MHz, the directional response is well behaved with the sensitivity decreasing with increasing angle and the variation across the angular range increasing with increasing frequency. At 10 MHz, the sensitivity drops approximately 6 dB for a 90° angle of incidence. Above 10 MHz the behavior changes significantly. The measurement at 13 MHz shows that the maximum sensitivity is no longer obtained at normal incidence, but at approximately $\pm$45°. At 15 MHz, the sensitivity appears to oscillate as a function of angle, but with a maximum drop in sensitivity of just 1.8 dB across the full 180° range. As the frequency is increased to 18 MHz, two large drops in sensitivity of greater than 25 dB appear in the response at approximately $\pm$30°. At 20 MHz, the nulls have reduced in magnitude but occur closer to normal incidence.

IV. THERMAL CHARACTERISTICS

The thermal performance of the sensor was characterized in terms of its sensitivity, linearity, and response time.

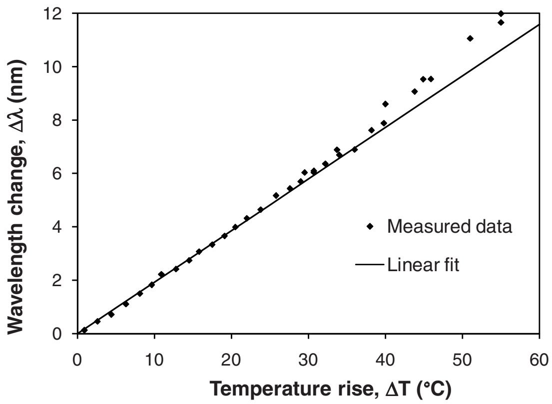

FIG. 9. Change in optimum bias wavelength as a function of temperature change.

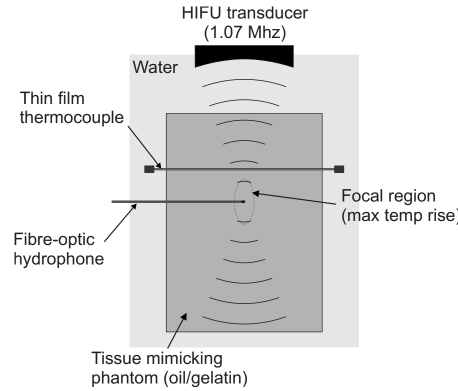

FIG. 10. Experimental setup for making simultaneous pressure and temperature measurements in a HIFU field.

A. Sensitivity

The sensitivity was measured by placing the tip of the fiber in a water bath at room temperature, T_0. The sensor was then placed into a second water bath held at second temperature, T_1, while the change in the optimum bias wavelength, $\Delta\lambda$, was recorded. The temperature change, $\Delta T = T_1 - T_0$, was measured using a pair of thermocouple probes in a differential measurement configuration. This was repeated for a range of values of T_1, from 25 °C to 80 °C, and the results can be seen in Fig. 9. In the linear region of the graph (up to $\Delta T = 45$ °C), a change of 1 nm in the bias wavelength corresponds to a temperature change of 5.18 °C. The photodiode noise-equivalent optical power is much less than the change in reflected power that occurs over a single wavelength tuning step. Hence, the temperature measurement resolution is determined largely by the minimum wavelength step by which the laser can be tuned, approximately 0.06 nm, which leads to a temperature resolution of approximately 0.34 °C.

B. Linearity and dynamic range

The calibration data in Fig. 9 show that the response of the hydrophone to temperature is linear up to a temperature change of approximately 45 °C, which in this case corresponds to a temperature of 70 °C. Above this, there is an increase in the gradient of the curve. This is consistent with a glass transition in the Parylene spacer. Below the glass transition temperature, T_g, the Parylene is in a hard, glassy state and acts elastically. In this state, the thermal expansion of the polymer is linear and reversible. Above T_g, the Parylene is in transition between glassy and rubbery moduli and viscoelastic losses are significant.[31] Hence the sensor is currently limited to measuring temperatures up to 70 °C.

C. Response time

The intrinsic thermal response time of the sensor, based on the time it takes for heat to diffuse across a 12 μm thick Parylene spacer, is approximately 850 μs.[22] However, the rate at which the system can measure temperature changes is limited by a combination of two factors: first, the acquisition rate of the USB A-D module which is used to sample the photodiode output, and second the overhead involved in communicating with the laser via the RS232 interface. These factors result in a system sampling rate of 200 samples/s for the temperature measurements. Since the system is only capable of measuring temperature in steps corresponding to the tuning resolution of the laser, there is a maximum temporal temperature gradient which the sensor can accurately measure. Since tuning one channel corresponds to a temperature change of approximately 0.34 °C, the maximum rate of temperature change which can be measured is approximately 67 °C s^{-1}.

V. MEASUREMENTS OF ULTRASOUND INDUCED HEATING

In order to demonstrate the applicability of the sensor for the measurement of ultrasound-induced heating, it was used to record the temperature rise produced at the focus of a HIFU transducer in a tissue mimicking phantom. These measurements were made at the National Physical Laboratory (NPL), Teddington, UK.

A. Experimental setup

The sensor was embedded in a tissue mimicking phantom based on an oil-gelatin emulsion,[5] as shown in Fig. 10. To provide a reference for the temperature measurement, a thin-film thermocouple (TFT) was also embedded within the phantom approximately 1 cm below the fiber-optic hydrophone. The TFT was developed at the UK's NPL in order to make accurate measurements of ultrasound-induced temperature rises.[5,6] The structure of the TFT renders it immune to heating artifacts such as viscous heating, to which wire thermocouples are susceptible.[4] The fiber-optic hydrophone was positioned such that the axis of the fiber was perpendicular to the acoustic axis. This removed the fiber mount from the acoustic path, thereby eliminating acoustic reflections from the mount. In order to compare the output of each device, a measurement was first made with the TFT at the focus. The system was then realigned (including changing the distance to the transducer) so that the fiber-optic hydrophone was at the focus and a second measurement made. The heating was induced by the output of a 1.07 MHz HIFU transducer with a focal length of 117 mm and a focal spot 3–4 mm in diameter and 4–5 cm in length (−6 dB). The heating was con-

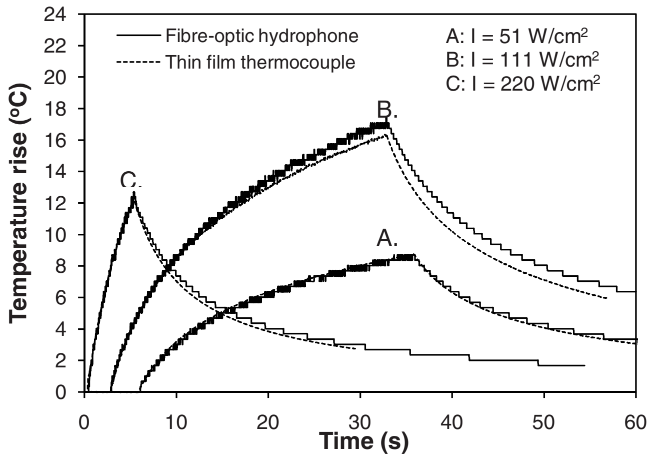

FIG. 11. Comparison of temperature-time curves obtained by the fiber-optic hydrophone and the thin-film thermocouple.

trolled by setting the intensity and duration of the (cw) insonation. It should be noted that intensity values quoted in the results below are based on values measured in water only. Thus they provide only an approximate indication of the values within the phantom.

B. Comparison of temperature-time curves measured by the fiber-optic hydrophone and thin-film thermocouple

In the first instance, a comparison of temperature-time curves obtained by both the fiber-optic hydrophone and the TFT, for a variety of acoustic output settings, was made. Figure 11 shows three temperature-time curves for acoustic intensities of 51, 111, and 220 W cm^{-2} (≈2.5, 3.7, and 5.4 MPa peak-to-peak pressures, respectively). The insonation at 220 W cm^{-2} was limited to 5 s in order to minimize the risk of damage to the TFT. It can be seen that the shape of the temperature-time curves measured by the fiber sensor closely match those measured by the TFT. This implies that there are no significant viscous heating artifacts in the measurement by the fiber-optic hydrophone. It can also be seen that in the case of the 111 W cm^{-2}, 30 s insonation, the maximum temperature measured by the sensor is slightly higher than that measured by the TFT. This is attributed to a slight error in the alignment of each sensor in the focal region of the beam. The overall shape remains a good match even in this case.

Additional measurements were made at a range of intensities as high as 700 W cm^{-2} (≈12 MPa peak-to-peak) which approaches clinical intensity levels. No damage or change in performance was observed at this intensity.

C. Simultaneous acquisition of ultrasound waveforms and a temperature-time curve

The arrangement shown in Fig. 10 was also used to demonstrate the ability of the system to conduct simultaneous acoustic and thermal measurements. The results can be seen in Fig. 12, which shows a temperature-time curve for a 30 s insonation with an acoustic intensity (I_{spta}—spatial peak, temporal average intensity) of 220 W cm^{-2} and several acoustic waveforms taken at different times during the insonation period. The temperature-time curve is of the same overall shape as those obtained for lower insonation intensities or shorter heating periods (Fig. 11) with the exception

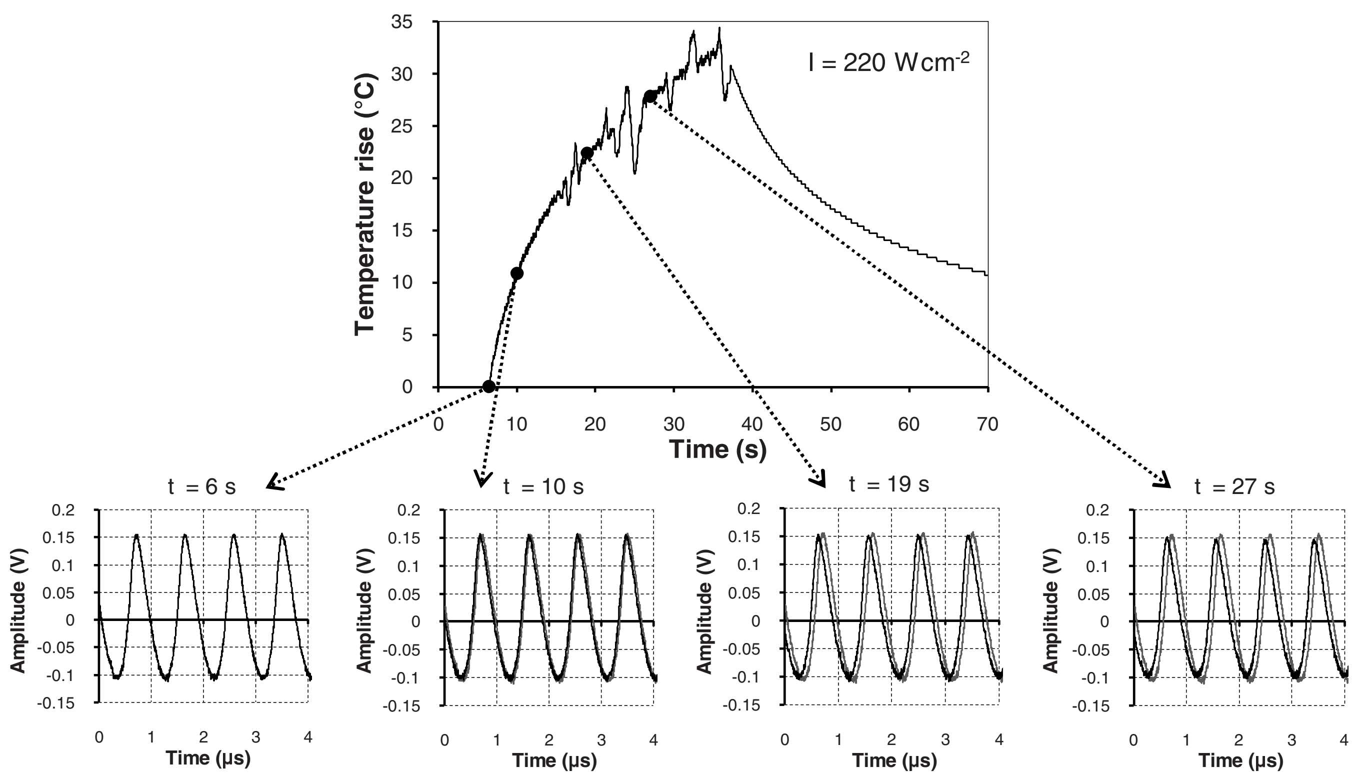

FIG. 12. Simultaneous acquisition of a temperature-time curve (top) and acoustic waveforms (lower row) captured at four different times during a 30 s insonation (cw). For the acoustic waveforms obtained at $t=10$, 19, and 27 s, the waveform captured at $t=6$ s (gray line) is also shown in order to illustrate the phase shift due to the thermally-induced change in sound speed.

that several rapid temperature fluctuations can be seen over the heating period. One possible explanation is that these fluctuations are related to the presence of cavitational activity close to the tip of the sensor. If bubbles form between the fiber-optic hydrophone and the transducer, some of the acoustic energy from the transducer will be reflected away from the sensor; this would lead to a temporary reduction in temperature. Similarly, if bubbles form behind the sensor, they may reflect some of the acoustic beam back toward the sensor thus increasing the local temperature. Cavitational activity close to the tip may also convert more acoustic energy to heat, thereby increasing the temperature temporarily while the activity persists.

The set of acoustic waveforms accompanying the temperature-time curve shows that as the temperature rises, the speed of sound increases slightly. The waveforms shift to the left of the trace, and the amplitude of the signal decreases slightly. These effects are expected since, in general, sound speed increases with temperature; thus the time-of-flight of the wave will be reduced. In addition, as the sound speed and the acoustic properties of the phantom change with temperature, the focal point of the transducer may move; thus the sensor will no longer be at the focus and the amplitude may decrease.

A limitation of the current system is that the acoustic waveforms were captured on a digitizing oscilloscope and transmitted to the control PC via a general purpose interface bus interface. With this method, it took approximately 2 s to instruct the scope to capture a waveform and download it to the PC. Thus, during the 30 s insonation used to obtain the data shown in Fig. 12, a maximum of only 15 acoustic waveforms could be captured. Unfortunately, none of these coincided with the rapid fluctuations in the temperature-time curve so it was not possible to test the above hypothesis that cavitational activity (which may have been evident from the acoustic waveforms) is responsible for these fluctuations. This limitation could be overcome by using an oscilloscope or PC digitizing card with an on-board segmented memory architecture. This would allow a large number of successive waveforms to be captured in real time, concatenated in a single segmented record, and the whole record downloaded to the PC in a single step as described in Ref. 32. A much higher waveform acquisition rate could then be achieved, enabling an acoustic waveform to be acquired for each measurement point on the temperature-time curve.

VI. CONCLUSIONS

A practical wideband (50 MHz) fiber-optic hydrophone system for characterizing diagnostic and therapeutic medical ultrasound fields has been demonstrated. In terms of acoustic performance, its principal advantage is that it can provide a small element size with significantly higher sensitivity than can be achieved with PVDF hydrophones of comparable element dimensions. As well as measuring acoustic pressure, the ability to measure temperature changes produced by ultrasound-induced heating has been demonstrated. There are two distinguishing features of this capability. First the measurement is free of errors due to viscous self-heating that afflict wire thermocouples conventionally used to make such measurements. Second, it is possible to acquire ultrasound waveforms while simultaneously monitoring the temperature. This unique dual measurement capability provides a means of directly correlating temperature rises with acoustic field parameters. For example, it could be employed to help understand the role that cavitation plays in enhancing tissue heating in HIFU therapy. A further advantage is that, unlike PVDF hydrophones, the fiber-optic hydrophone appears to be able to withstand the hostile environment produced by a HIFU field at clinical intensity levels. Even if it should fail, the ability to batch fabricate the sensors at low unit cost using all vacuum deposition techniques means that the sensor can be inexpensively replaced. Other advantages include small physical size and flexibility, biocompatibility, and electrical passivity, attributes that suggest the sensor could be used as an implantable probe for making *in-vivo* measurements.

Future work will be directed toward improving both the acoustic and thermal performance of the hydrophone. Preliminary experimental and theoretical studies suggest that there is significant scope to obtain a more uniform frequency response by appropriately shaping the tip of the optical fiber to reduce the influence of diffraction.[24] This also offers the prospect of producing an improved directional response, particularly at higher frequencies where the fluctuations in angular sensitivity are most apparent. Although the current NEP of 15 kPa is sufficient for many medical ultrasound measurement applications, there is significant scope to increase sensitivity if required. The noise performance of the current system is limited by the relatively high phase noise of the SG-DBR interrogation laser. It has previously been shown that the use of an external cavity laser as the interrogation source, which has significantly narrower linewidth and therefore lower phase noise, can provide a NEP of 3 kPa.[33] There is further potential to reduce the NEP by replacing the gold coatings currently used to form the mirrors of the FPI with dielectric coatings. These are significantly less absorbing enabling a higher finesse FPI to be obtained. A NEP of 0.21 kPa has been achieved with free-space illuminated sensors fabricated in this way.[34]

The sensor is currently limited to making temperature measurements up to 70 °C and the thermal resolution is limited by the wavelength tuning resolution of the laser. The former may be improved by using an alternative material to form the spacer, such as the Parylene variant Parylene-HT. This material offers similar optical and acoustic properties to Parylene-C but with a higher glass transition temperature. The thermal resolution may be increased by monitoring the variation in the reflected power and using this data, along with knowledge of the ITF, to interpolate between successive wavelength tuning steps. It should then be possible to achieve a resolution limited by the photodiode noise voltage rather than tuning resolution of the laser.

In summary, it is considered that the wide bandwidth, small element size, and high sensitivity of this type of sensor, along with its ability to measure temperature, offers a potentially useful new measurement tool for characterizing medical ultrasound fields.

ACKNOWLEDGMENTS

This work was funded by the UK Engineering and Physical Sciences Research Council (EPSRC). The authors acknowledge the support of the National Measurement System Programme Unit of the UK Department for Innovation, Universities and Skills (DIUS) for the work carried out at NPL.

[1] G. Harris, "Progress in medical ultrasound exposimetry," IEEE Trans. Ultrason. Ferroelectr. Freq. Control **52**, 717–736 (2005).

[2] W. J. Fry and R. B. Fry, "Determination of absolute sound levels and acoustic absorption coefficients by thermocouple probes—Theory," J. Acoust. Soc. Am. **26**, 294–310 (1954).

[3] C. C. Coussios, C. H. Farny, G. T. Haar, and R. A. Roy, "Role of acoustic cavitation in the delivery and monitoring of cancer treatment by high-intensity focused ultrasound (HIFU)," Int. J. Hyperthermia **23**, 105–120 (2007).

[4] H. Morris, I. Rivens, A. Shaw, and G. ter Haar, "Investigation of the viscous heating artefact arising from the use of thermocouples in a focused ultrasound field," Phys. Med. Biol. **53**, 4759–4776 (2008).

[5] D. R. Bacon and A. Shaw, "Experimental validation of predicted temperature rises in tissue-mimicking materials," Phys. Med. Biol. **38**, 1647–1659 (1993).

[6] A. Shaw, N. M. Pay, R. C. Preston, and A. D. Bond, "Proposed standard thermal test object for medical ultrasound," Ultrasound Med. Biol. **25**, 121–132 (1999).

[7] IEC, "IEC62306 Ultrasonics-field characterization-test objects for determining temperature elevation in diagnostic ultrasound fields," International Electrotechnical Commission, Geneva, 2006.

[8] R. L. Phillips, "Proposed fiberoptic acoustical probe," Opt. Lett. **5**, 318–320 (1980).

[9] J. Staudenraus and W. Eisenmenger, "Fiberoptic probe hydrophone for ultrasonic and shock-wave measurements in water," Ultrasonics **31**, 267–273 (1993).

[10] C. Wurster, J. Staudenraus, and W. Eisenmenger, "The fiber optic probe hydrophone," Proc.-IEEE Ultrason. Symp. **2**, 941–944 (1994).

[11] P. A. Lewin, S. Umchid, A. Sutin, and A. Sarvazyan, "Beyond 40 MHz frontier: The future technologies for calibration and sensing of acoustic fields," J. Phys.: Conf. Ser. **1**, 38–43 (2004).

[12] J. E. Parsons, C. A. Cain, and J. B. Fowlkes, "Cost-effective assembly of a basic fiber-optic hydrophone for measurement of high-amplitude therapeutic ultrasound fields," J. Acoust. Soc. Am. **119**, 1432–1440 (2006).

[13] V. A. Leitao, W. N. Simmons, Y. F. Zhou, J. Qin, G. Sankin, F. H. Cocks, J. Fehre, B. Granz, R. Nanke, G. M. Preminger, and P. Zhong, "Comparison of light spot hydrophone (LSHD) and fiber optic probe hydrophone (FOPH) for lithotripter field characterization," Renal Stone Disease **900**, 377–380 (2007).

[14] V. Wilkens and C. Koch, "Fiber-optic multilayer hydrophone for ultrasonic measurement," Ultrasonics **37**, 45–49 (1999).

[15] V. Wilkens, "Characterization of an optical multilayer hydrophone with constant frequency response in the range from 1 to 75 MHz," J. Acoust. Soc. Am. **113**, 1431–1438 (2003).

[16] V. Wilkens, C. Wiemann, C. Koch, and H. J. Foth, "Fiber-optic dielectric multilayer temperature sensor: In situ measurement in vitreous during Er:YAG laser irradiation," Opt. Laser Technol. **31**, 593–599 (1999).

[17] P. C. Beard and T. N. Mills, "Extrinsic optical-fiber ultrasound sensor using a thin polymer film as a low-finesse Fabry–Pérot interferometer," Appl. Opt. **35**, 663–675 (1996).

[18] P. C. Beard and T. N. Mills, "Miniature optical fibre ultrasonic hydrophone using a Fabry–Pérot polymer film interferometer," Electron. Lett. **33**, 801–803 (1997).

[19] Y. Uno and K. Nakamura, "Pressure sensitivity of a fiber-optic microprobe for high-frequency ultrasonic field," Jpn. J. Appl. Phys., Part 1 **38**, 3120–3123 (1999).

[20] P. Beard, A. Hurrell, and T. Mills, "Characterization of a polymer film optical fiber hydrophone for use in the range 1 to 20 MHz: A comparison with PVDF needle and membrane hydrophones," IEEE Trans. Ultrason. Ferroelectr. Freq. Control **47**, 256–264 (2000).

[21] J. M. Vaughan, *The Fabry–Pérot Interferometer: History, Theory, Practice and Applications* (Hilger, London, 1989).

[22] J. G. Laufer, P. C. Beard, S. P. Walker, and T. N. Mills, "Photothermal determination of optical coefficients of tissue phantoms using an optical fibre probe," Phys. Med. Biol. **46**, 2515–2530 (2001).

[23] P. Morris, P. Morris, A. Hurrell, E. Zhang, S. Rajagopal, and P. Beard, "A Fabry–Pérot fibre-optic hydrophone for the measurement of ultrasound induced temperature change," Proc.-IEEE Ultrason. Symp. , 536–539 (2006).

[24] P. Morris, "A Fabry–Pérot fibre-optic hydrophone for the characterisation of ultrasound fields," Ph.D. thesis, University College London, London (2008).

[25] B. T. Cox and P. C. Beard, "The frequency-dependent directivity of a planar Fabry–Pérot polymer film ultrasound sensor," IEEE Trans. Ultrason. Ferroelectr. Freq. Control **54**, 394–404 (2007).

[26] P. C. Beard, F. Perennes, E. Draguioti, and T. N. Mills, "Optical fiber photoacoustic-photothermal probe," Opt. Lett. **23**, 1235–1237 (1998).

[27] K. Nakamura and K. Nimura, "Measurements of ultrasonic field and temperature by a fiber optic microprobe," J. Acoust. Soc. Jpn. E **21**, 267–269 (2000).

[28] SCS, "Parylene properties," www.scscoatings.com (2008), URL http://www.scscoatings.com/docs/coatspec.pdf (date last viewed 4/20/09).

[29] Z. Y. Zhang, P. Zhao, P. Lin, and F. G. Sun, "Thermo-optic coefficients of polymers for optical waveguide applications," Polymer **47**, 4893–4896 (2006).

[30] R. A. Smith and D. R. Bacon, "A multiple-frequency hydrophone calibration technique," J. Acoust. Soc. Am. **87**, 2231–2243 (1990).

[31] R. O. Ebewele, *Polymer Science and Technology* (CRC, Boca Raton, FL, 1996).

[32] E. Z. Zhang and P. Beard, "Broadband ultrasound field mapping system using a wavelength tuned, optically scanned focused laser beam to address a Fabry–Pérot polymer film sensor," IEEE Trans. Ultrason. Ferroelectr. Freq. Control **53**, 1330–1338 (2006).

[33] P. Morris, P. Beard, and A. Hurrell, "Development of a 50 MHz optical fibre hydrophone for the characterisation of medical ultrasound fields," Proc.-IEEE Ultrason. Symp. **3**, 1747–1750 (2005).

[34] E. Zhang, J. G. Laufer, and P. Beard, "Backward-mode multiwavelength photoacoustic scanner using a planar Fabry–Pérot polymer film ultrasound sensor for high resolution three-dimensional imaging of biological tissues," Appl. Opt. **47**, 561–577 (2008).